HTTR 3-D Cross-Section Generation with Serpent and MAMMOTH

Vincent Laboure, Javier Ortensi, and Andrew Hummel

September 2018

INL

Idaho National Laboratory

HTTR 3-D Cross-Section Generation with Serpent and MAMMOTH

Vincent Laboure, Javier Ortensi, and Andrew Hummel

September 2018

Idaho National Laboratory
INL ART Program
Idaho Falls, Idaho 83415

http://www.inl.gov

INL ART Program

HTTR 3-D Cross-Section Generation with Serpent and MAMMOTH

INL/EXT-18-51317
Revision 0

September 2018

Author:

_____   9/18/18
Vincent Laboure, Staff Scientist   Date

Technical Reviewer: (Confirmation of mathematical accuracy, and correctness of data and appropriateness of assumptions.)

_____   9/18/18
Sebastian Schunert, Staff Scientist   Date

Approved by:

_____   9/18/18
Diane V. Croson   Date
INL ART Deputy Director

_____   9/18/18
Hans D. Gougar   Date
ART Director
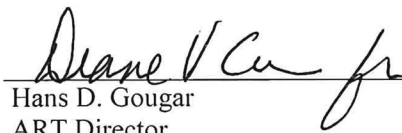
_____   9/18/18
Michelle T. Sharp   Date
INL Quality Engineer

REVISION LOG

Rev.	Date	Affected Pages	Revision Description
0	09/19/2018	All	New document
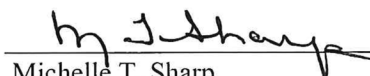
ABSTRACT

The High Temperature Test Reactor (HTTR) is a graphite-moderated thermal reactor with a nominal power output of 30 MWth. The purpose of this work is to prepare a set of neutron cross sections for use in the transient analyses of three Loss of Forced Cooling (LOFC) events planned for this reactor. The cross sections are generated with the Serpent 2 3-D Monte Carlo code to include the axial heterogeneity and the strong axial coupling of this core. The approach yields good agreement of results when compared to previously used 2-D lattice models, which require a fine spatial discretization and, surprisingly, comes at a higher computational cost. In addition, the temperature distribution must be considered to obtain reasonable cross sections and the axial leakage component dominates the spectral effects in the core. Consequently, a temperature model as a function of the fuel and moderator temperatures is adopted, and the core is depleted to 390 effective full-power days (EFPDs). A full tabulation of cross sections is prepared at this burnup point for a variety of fuel and moderator temperatures. Next, the multiphysics reactor application MAMMOTH is used to evaluate the quality of these cross sections using a diffusion solver. As expected, the homogenization error in the cross sections is significant and the Super Homogenization (SPH) correction from MAMMOTH is necessary to preserve key reaction rates. The SPH-corrected MAMMOTH results are in excellent agreement with the Serpent results and reproduce both the reference power profile and temperature coefficients at each tabulation point. This fact confirms the accuracy of the SPH-corrected cross sections and demonstrates the maturity of using Serpent 2 and MAMMOTH for 3-D cross-section generation, even for reactors as complex as the HTTR. Finally, the authors recommend that the cross sections should be parametrized with the local burnup and that a full core burnup calculation with coupled thermal-fluids would provide a better estimate of the initial condition for any subsequent transient analysis. Unfortunately, this was not within the scope of this work, and direct analysis with these tabulations should be considered as a first-order approximation, at best.

CONTENTS

FIGURES

TABLES

ACRONYMS

ART	Advanced Reactor Technologies
BP	burnable poison
BU	burnup
CR	control rod
EFPD	effective full power day
eV	electron-volt
HTGR	High Temperature Gas Reactor
HTTR	High Temperature Test Reactor
JAEA	Japan Atomic Energy Agency
LOFC	loss of forced cooling
LWR	Light Water Reactor
MCNP	Monte Carlo N-Particle Transport Code
MOOSE	Multiphysics Object Oriented Simulation Environment
RMS	root mean square
RR	replaceable reflector
SPH	super homogenization
TRISO	tristructural isotropic
UO_2	uranium dioxide

HTTR 3-D Cross-Section Generation with Serpent and MAMMOTH

1. INTRODUCTION

The High Temperature Engineering Test Reactor (HTTR) is a graphite-moderated, helium-cooled reactor developed by the Japan Atomic Energy Research Institute, now the Japan Atomic Energy Agency (JAEA). Built at the Oarai Research and Development Center, this advanced reactor first reached criticality in November 1998, followed by full-power operation on December 7, 2001 [1]. Designed and built to further establish High Temperature Gas Reactor (HTGR) technologies, the core has been central to many reactor physics experiments [2,3,4,5] and safety studies [6,7]. Additionally, the core configuration and experiments have been extensively benchmarked [8,9,10]. Operated at a nominal power output of 30 MWth, this one-of-a-kind reactor offers many advantages over the typical light water reactor (LWR). For instance, the tristructural isotropic (TRISO) fuel particles are developed to inherently retain all fission products, and the graphite core allows for much higher output temperatures. However, they also add challenges in the numerical modeling of these systems. The doubly heterogeneous nature of the TRISO particles arising from the multiple coated layers ultimately leads to the need of special treatments for the proper generation of cross sections with deterministic methods. In addition, the random nature of these particles can present further difficulties. Several codes, such as SCALE [11] and DRAGON [12], have successfully addressed this issue. Also, unlike LWRs that tend to have localized effects, the much larger neutron migration area in the HTTR leads to a highly coupled core. This makes the task of including long-range spectral effects in lattice calculations particularly difficult. However, supercell calculations have proven successful [13], although these tend to require large amounts of computation time [14] to achieve respectable results when compared to 2-D Monte-Carlo calculations. Finally, the core has a very high temperature gradient when operating at full power, thus essentially nullifying any isothermal assumptions. In addition, the core is highly heterogeneous, even at the fuel block level. Several key findings from previous work [13] led to the conclusions that 3-D cross-section preparation is crucial to resolve the heterogeneity problems. Current improvements in the Serpent 2 [15] Monte-Carlo code allow depletion calculations with a full-core configuration; therefore, a fully explicit HTTR model was constructed and depleted to 390 effective full-power days (EFPDs). The ENDF/B-VII.0 neutron cross section libraries are used to perform comparisons to the Monte Carlo N-Particle Transport Code (MCNP) reference model while ENDF/B-VII.1 libraries are used in the depletion and the cross-section preparation.

As part of a cooperative effort between Japan and the United States under the Civil Nuclear Energy Working Group, the Advanced Reactor Technologies (ART) Program at INL and JAEA are participating in a multi-national research project sponsored by the Nuclear Energy Agency of the Organization of Economic Cooperation and Development. Three pressurized loss of forced cooling (LOFC) tests are being performed at the HTTR to confirm the ability of the core to shut down and safely reject heat in the event of a circulator trip, without control rods being inserted. These events are classified as anticipated transients without scram. The first of the experiments was completed on December 21, 2010, at 9 MW (30% of rated power), with data provided by JAEA to participating countries (including the U.S.) to be used for system code/model validation. The LOFC#2 (30 MW) and LOFC#3 (9 MW with loss of Vessel Cooling System) experiments are tentatively scheduled to be completed in 2019. The present work focuses on generating the cross-sections to be used in any multiphysics code that is able to compute a more accurate temperature profile than that originally included in the Serpent2 model.

The current approach entails the computation of 3-D multigroup cross sections at various state points for the variables that are deemed to have a significant impact on the cross section. This is followed by the application of the Super Homogenization (SPH) method [16,17] to correct the homogenized cross sections. This enables the undertaking of transient simulations such as the HTTR LOFC events. Two

LOFC cases are primarily considered in the preparation of cross sections in this work: one starting at 9 MW and another at 30 MW.

This report is organized as follows: Section 2 describes and verifies the Serpent 2 3-D HTTR model against the Monte-Carlo N-Particle (MCNP) [18] continuous energy code. Based on this model, a study regarding the importance of the core temperature distribution is performed in Section 3 to determine how the cross sections should be functionalized. It is noted that the functionalization is only done at 390 EFPD, assuming a fixed temperature distribution during the entire depletion calculation. A more accurate approach would be to also tabulate cross sections at each depletion step and to create a library depending on temperature and the local burnup. This would then allow to repeat the depletion calculation using a more accurate temperature distribution. Although it is likely that this local burnup may also be of significant importance, since the LOFC transient and the time to recriticality are highly dependent on the initial xenon concentrations, which in turn depend on the local flux level [19], the cross sections are not considered to depend thereon in this report (mostly due to time constraint). The approximated temperature profile as well as the tabulation points are also described Section 3. At that point, the cross sections have been generated by Serpent2 with postprocessing steps being done by MAMMOTH [20], the general reactor physics application based on the Multiphysics Object Oriented Simulation Environment (MOOSE) [21]. In Section 4, the homogenization error stemming from the cross section is evaluated, emphasizing the need for SPH correction. This is performed within MAMMOTH, whose SPH procedure relies on the Preconditioned Jacobian-Free Newton-Krylov method [17]. Drastically improved results for both the temperature coefficients and power profile compared to the uncorrected cross sections are presented for both the 9-MW and 30-MW LOFC. Final conclusions and the identification of future work are discussed in Section 5.

2.   MODEL DESCRIPTION AND VERIFICATION

2.1   Model Comparison

The Serpent 2 model is derived from the most recent criticality benchmark evaluation [10], which uses MCNP. To compare equivalent models, both the MCNP (using v6.1.1) and Serpent 2 models are modified accordingly to make them closer to reality (and as close to each other as possible):

1. The MCNP benchmark model assumes a burnable poison (BP) pitch equal to the fuel pin pitch, when the BPs are actually offset. The pitch is appropriately calculated and changed in both models.

2. Fuel handling holes are not modeled in the benchmark, but rather the graphite density is adjusted. Due to the complex geometry, a volume equivalent cylinder is instead added to all fuel blocks, removable reflectors, and control rod (CR) blocks in both models.

3. The benchmark contains a graphite overcoat on the TRISO fuel, but the process of generating the random particle distribution file in Serpent 2 does not permit adding this; therefore, it is removed.

4. Unlike MCNP, Serpent 2 has the capability of randomly distributing the TRISO particles in the fuel pins, and all of the depletion analysis presented in this report use that feature. A homogenous mixture of 7.9 wt.% UO_2 and graphite matrix is used in all of the fuel pins to compare against the MCNP model.

The eigenvalues are first compared at the fuel block level using specular boundary conditions everywhere to verify geometry and axial material distributions. This is very important because neither fuel nor BPs span the entire block length. Helium and graphite gaps are at the ends of the fuel, and the BP channels are loaded with a 10-cm graphite zone splitting the BP in half as shown in Figure 1.

13
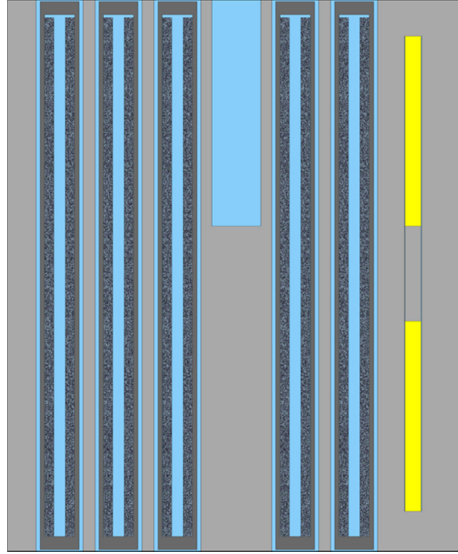
Figure 1. Axial view of a standard HTTR fuel block with fuel (dark grey), He (blue), and BP (yellow).

Table 1 lists the eigenvalues for the different cases, and excellent agreement is observed at the block level. Next, the four different types of fuel columns or block stacks are examined. Each column consists of nine blocks: two lower replaceable reflector (RR) blocks, five central fuel blocks, and two upper RR blocks. The lower and upper two fuel blocks for each stack are the same; these different stacks are shown in Figure 2 and a radial view of the core layout is shown in Figure 3. Again, there is an excellent agreement at the column level. The next check is to examine a supercell consisting of the central CR column surrounded by six fuel columns as seen in Figure 4. Due to how boundary conditions can be applied between the two codes, the supercell is placed into a helium-filled cylinder with specular boundary conditions and the results differ by only 10 pcm. Full core models are then compared with the CRs fully inserted, fully withdrawn, and at the cold critical condition heights [8] (note however that the core is not critical in that latter case because of the homogeneous enrichment chosen for this code-to-code comparison). The largest difference in the core eigenvalue is only 52 pcm and occurs with all rods fully inserted. This difference is most likely a reflection of the different particle tracking methods employed in the two codes, as Serpent 2 uses a combination of traditional surface-tracking and the Woodcock delta-tracking methods. Ultimately, the models are in good agreement.

Table 1. MCNP6.1 and Serpent 2 eigenvalue comparisons using ENDF/B-VII.0 (293 K).

Models (homogenized	MCNP6.1	Serpent 2	Δpcm
Fuel block	1.23597 ± 0.00001	1.23591 ± 0.00006	-6
Fuel columns	1.23422 ± 0.00003	1.23425 ± 0.00006	+3
Supercell (rods in)	1.13782 ± 0.00003	1.13777 ± 0.00006	-5
Supercell (rods out)	1.34230 ± 0.00003	1.34220 ± 0.00004	-10
Full-core (rods in)	0.86089 ± 0.00002	0.86141 ± 0.00006	-52
Full-core (rods out)	1.22328 ± 0.00002	1.22365 ± 0.00004	-37
Full-core (critical)	1.17790 ± 0.00003	1.17754 ± 0.00004	36

Stack 1	Stack 2	Stack 3	Stack 4
RR	RR	RR	RR
RR	RR	RR	RR
6.7/2.0	**7.9**/2.0	**9.4**/2.0	**9.9**/2.0
5.2/2.5	**6.3**/2.5	**7.2**/2.5	**7.9**/2.5
4.3/2.5	**5.2**/2.5	**5.9**/2.5	**6.3**/2.5
3.4/2.0	**3.9**/2.0	**4.3**/2.0	**4.8**/2.0
3.4/2.0	**3.9**/2.0	**4.3**/2.0	**4.8**/2.0
RR	RR	RR	RR
RR	RR	RR	RR

Figure 2. Four different HTTR fuel columns/stacks (fuel/BP wt.% enrichment). The axial slices are indexed from 1 (top) to 9 (bottom).
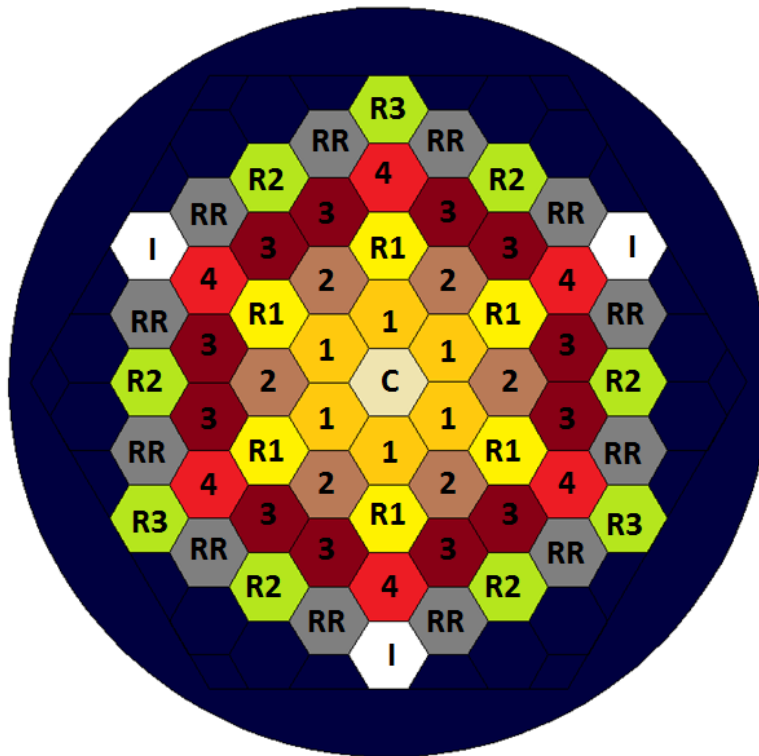
Figure 3. HTTR core layout with fuel positions (Stacks 1–4), control rods (C, R1, R2, R3), replaceable reflectors (RR), and instrumentation (I).
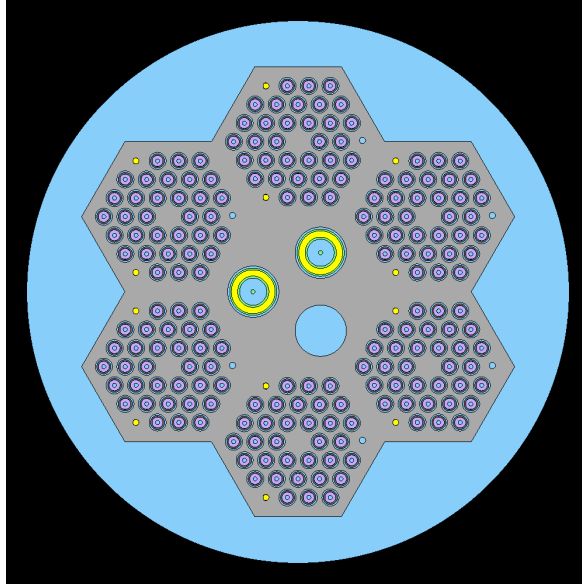
Figure 4. Supercell arrangement with central CR column surrounded by six fuel columns.

2.2   Model Overview and Methodology

Table 2 lists the main HTTR core design specifications and Table 3 gives an overview of the fuel form characteristics. There is a total of 12 different fuel enrichments in the 150 fuel blocks. Due to both memory and computational limitations, the core is depleted at the fuel block level. The depletion steps and corresponding burnup (BU) limits are shown Table 4. The predictor-corrector method is used for the time integration. A xenon equilibrium option was chosen to start.

Table 2. Main HTTR design specifications.

Thermal Power (MW)	30
Outlet Coolant Temperature (°C)	850–950
Inlet Coolant Temperature (°C)	395
Primary Coolant Pressure (MPa)	4
Core Structure	Graphite
Equivalent Core Diameter (m)	2.3
Effective Core Height (m)	2.9
Average Power Density (W/cm^3)	2.5
Fuel/Enrichment	UO_2 / 3–10 wt.%
Fuel Type	Pin-in-Block
Burn-Up Period (EFPDs)	660
Coolant Material/Flow	Helium Gas / Downward
Reflector Thickness: Top/Side/Bottom (m)	1.16/0.99/1.16
Number of Fuel Assemblies	150
Number of Fuel Columns	30
Number of Control Rod Pairs: In Core/In Reflector	7/9

Table 3. Main HTTR fuel specifications.

Fuel Kernel	
Material	UO$_2$
Diameter (μm)	600
Density (g/cm^3)	10.41
Coated Fuel Particle	
Type/Material	TRISO
Diameter (μm)	920
Impurity (ppm)	<3 (Boron Equivalent)
Fuel Compact	
Type	Hollow Cylinder
Material	CFPs, Binder, and Graphite
Outer/Inner Diameter (cm)	2.6/1.0
Length (cm)	3.9
Packing Fraction of CFPs (vol%)	30[a] (A and B-3)
	35 (B-1 and B-2)
Density of Graphite Matrix (g/cm^3)	1.7
Impurity in Graphite Matrix (ppm)	<1.2 (Boron Equivalent)
Fuel Rod	
Outer Diameter (cm)	3.4
Sleeve Thickness (mm)	3.75
Length (cm)	54.6
Number of Fuel Compacts	14
Number of Rods in a Block	31/33
Graphite Sleeve	
Type	Cylinder
Material	IG-110 Graphite
Length (cm)	58
Gap Width between Compact and Sleeve (mm)	0.25
Graphite Block	
Type/Configuration	Pin-in-Block/Hexagonal
Material	IG-110 Graphite
Width across Flats (cm)	36
Height (cm)	58
Fuel Hole Diameter (cm)	4.1
Density (g/cm^3)	1.75
Impurity (ppm)	<1 (Boron Equivalent)
a. Only A-Type fuel with a packing fraction of 30 is used in this study.	

Table 4. Burnup steps chosen the depletion calculation in days and MWd/kgU with the reactor operating at 30 MW.

Steps	Burnup (days)	Burnup (MWd/kgU)
0	0	0
1	1	0.03
2	10	0.33
3	60	2.00
4	110	3.67
5	160	5.34
6	210	7.00
7	260	8.67
8	310	10.34
9	360	12.01
10	390	13.01

The position of the control rods C, R1, and R2 (see Figure 3) depends on the power of the core. For the 30-MW steady-state, they are 277.0 cm withdrawn. For 9 MW, the temperature of the core is lower and less reactivity should be inserted for a critical core configuration, which is why the control rods are only 227.2 cm withdrawn. On the other hand, the control rod C3 is only used for shutdown margin and is fully withdrawn in both cases (406.0 cm). In this report, the reactor is assumed to have been operated at 30 MW for 390 EFPDs. The detailed power history of the HTTR core was not implemented in the depletion sequence as it was not available. The steady-state starting points for two LOFC transients are considered: (1) one starting at 30 MW, and (2) another one starting at 9 MW, assuming that equilibrium for I-135 and Xe-135 has been reached.

3. 3-D CROSS-SECTION GENERATION

In this section, the functionalization of the cross section is presented. It is noted that it is only done at 390 EFPD, assuming a fixed temperature distribution during the entire depletion calculation. A more accurate approach would be to also tabulate cross-sections at each depletion step and to create a library depending on temperature and the local burnup. This would then allow to repeat the depletion calculation using a more accurate temperature distribution. Although it is likely that this local burnup would be of significant importance – since the LOFC transient and the time to recriticality are highly dependent on the initial xenon concentrations, which in turn depend on the local flux level [18], the cross-sections are not considered to depend thereon in this report (mostly due to time constraint). This constitutes an approximation because a more sophisticated depletion and temperature model (e.g. through multiphysics coupling) will result in different local burnups throughout the core and thus a different initial condition for the subsequent transients.

3.1 Energy Structure

The energy structure chosen for the HTTR is one that was successfully used for the Transient Reactor Test Facility [22] with the fastest two energy groups combined to improve statistics. The energy bounds are summarized in Table 5. This structure is used for both the multigroup cross-section generation and to determine the power profile from Serpent 2.

Table 5. Energy bounds in eV of the ten energy groups of index g.

g	10	9	8	7	6	5	4	3	2	1
Lower	1.00E-5	2.00E-2	4.73E-2	7.65E-2	2.10E-1	6.25E-1	8.10E+0	1.33E+2	3.48E+3	1.16E+5
Upper	2.00E-2	4.73E-2	7.65E-2	2.10E-1	6.25E-1	8.10E+0	1.33E+2	3.48E+3	1.16E+5	4.00E+7

3.2   Temperature Influence on the Core

A preliminary study was performed to show that the influence on the multiplication factor of the moderator and fuel temperature radial distribution was not significant compared to that of their respective axial distribution. For that reason, the cross-section library is generated for temperature profiles, which only have axial dependency.

3.3   Temperature Model

Using an isothermal temperature model in the 3-D simulation yields significant discrepancies in the cross sections. This is not only because of the large axial temperature gradients in the core but also because of its strong axial coupling. The general approach is to establish an approximate temperature profile to be used throughout the transient. Given average moderator and fuel temperatures, this profile is applied to obtain local temperatures in each axial slice of the core and used to run the Serpent 2 calculations. The interpolation of the cross-sections during the transient is also done using the local temperatures. An assumption implied by this methodology is thus that the temperature distribution change over time does not affect the cross sections tabulated at steady-state temperatures.

More specifically, since Serpent 2 is not coupled to any other code to obtain an accurate temperature profile, it is necessary to make approximations. Besides, in an effort to minimize the computational burden of each individual Serpent 2 calculation, it is found that limiting the number of distinct temperatures for both moderator and fuel is crucial. Therefore, it is essential to accurately (1) bound the fuel and moderator temperatures during the 9-MW and 30-MW LOFC transients to make sure the temperature state points include all the temperatures encountered during the transient; and (2) predict the axial temperature profile.

To address the first point, the 9-MW transient shown in Figure 5 is considered. Several points clearly appear that can be reasonably assumed to hold for the 30-MW case: the increase in fuel temperature after LOFC is very limited, due to the strongly negative fuel temperature coefficient, and the moderator temperature never exceeds the fuel temperature. These two properties are also assumed to be true at any spatial location of the core.

To address the second, the 9-MW and 30-MW steady-state temperature distributions from [23] are considered. Then the temperature profiles are determined as follows:

1. The temperature shape is assumed to be time-independent throughout the transient. Although heat conduction and radiation tend to make the distribution flatter when no heat is generated, the decay heat distribution has a similar profile as the power since the fission product concentration is closely related to the number of fissions having occurred there. Furthermore, the large graphite heat capacity implies that heat diffusion is a relatively slow process. Since the shapes for the 9-MW and 30-MW steady-state temperature distributions are fairly similar, the latter shape is selected for both cases. Note however, that while this is a good approximation for the fuel temperature, it is a little more questionable for the moderator temperature since its gradient gets larger as the power increases. This does not constitute a limitation of the method but was mainly done because of time constraint.

2. To minimize the number of distinct temperatures used in the Serpent 2 calculations that rapidly become expensive, slices with similar temperatures (using engineering judgement) are assigned to their average. For the moderator, Slices 1 to 3 are then combined, Slice 4 is considered individually,

and Slices 5 to 9 are grouped together (see Figure 2). For the fuel, Slice 3 is considered on its own while Slices 4 to 7 are combined (Slices 1, 2, 8, and 9 do not contain any fuel). In summary, for each set of average fuel and moderator temperatures (T_f, T_m), only two axial values are used to represent the spatial shape of the fuel temperature and three for the moderator.

3. If after applying the profile, the fuel or moderator temperature drops below 294 K, it is set to 294 K because: (1) it is the lowest temperature point available in the current continuous energy libraries, and (2) temperatures below that value would be unphysical.
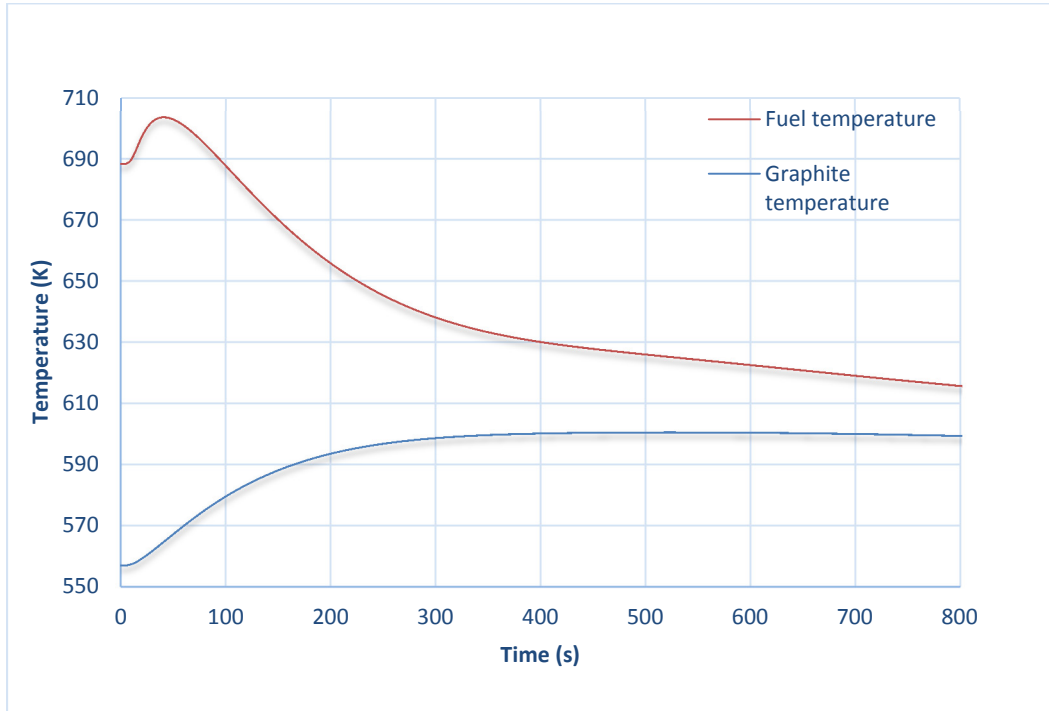
Figure 5. Average temperature evolution for the 9-MW LOFC from [23].

As an example, Figure 6 shows the temperature profile that is chosen for the fuel and moderator average temperatures set to 900 K and 600 K, respectively. In particular, the fuel temperature is only considered between Slices 3 and 7 because the other slices contain only reflector blocks.

The libraries for the 9-MW and 30-MW transients are generated independently because the equilibrium isotopic concentrations (in particular the poison concentrations) are different in both cases, due to the different control rod positions. Therefore, to minimize computational costs, state points are considered separately for both transients.
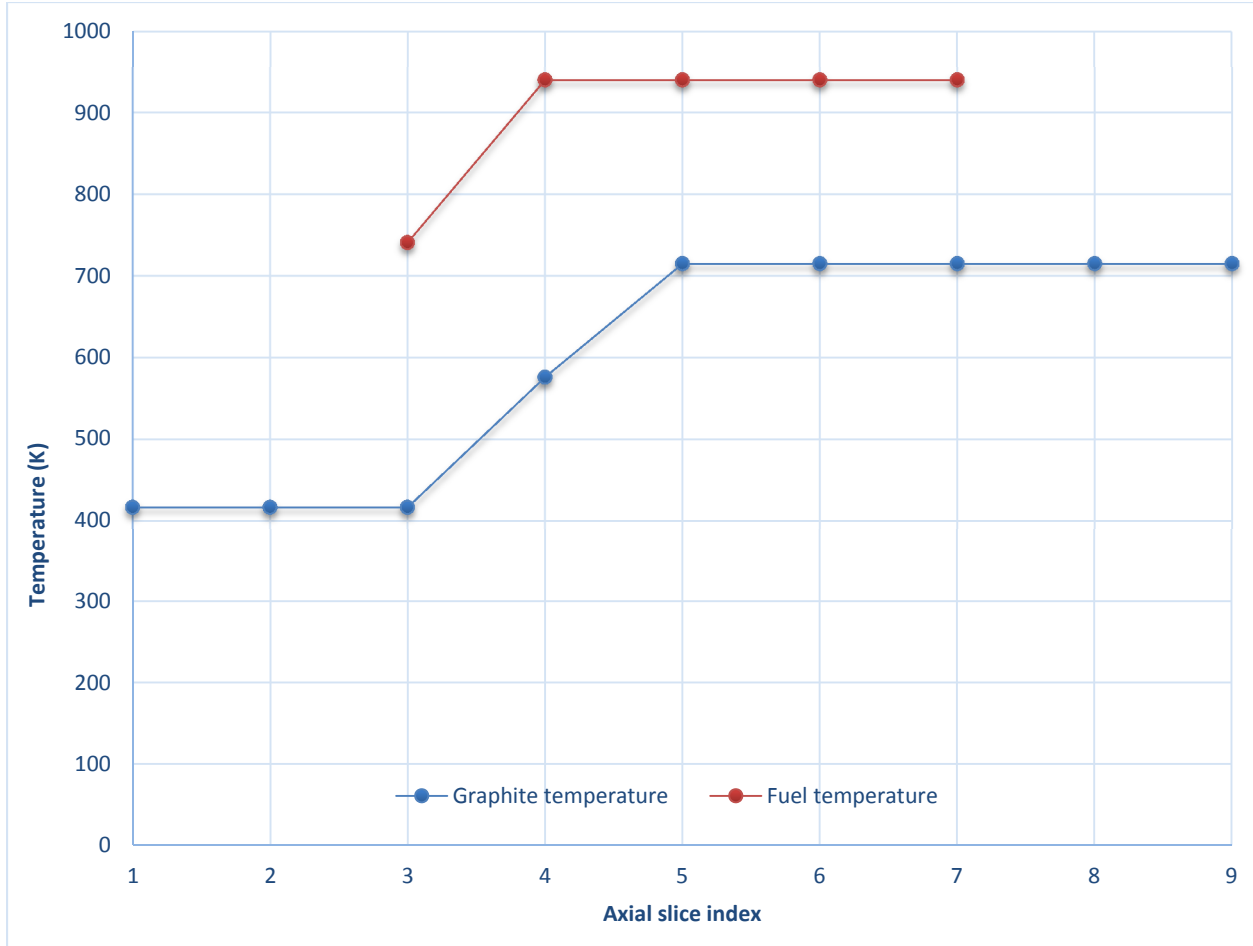
Figure 6. Example of the few-point approximated temperature profiles used in Serpent 2 for fuel and moderator average temperatures of 900 K and 600 K, respectively. The slice index goes from 1 (top) to 9 (bottom).

3.4   State Points

Table 6 and Table 7 show all the table points that are selected for the fuel and moderator temperatures for the 30-MW and 9-MW transients, respectively. Because of our assumption that the moderator temperature never exceeds that of the fuel, a lot of cases are not physical and, thus, are ignored. Nevertheless, as seen on Figure 6, the ratio of the minimum temperature to the average temperature is smaller for the moderator than for the fuel. The implication is that for instance if T_f and T_m are 600 K and 700 K, respectively, the value for T_m in Slice 3 is still lower than that of T_f in that same slice. This is why some state points with an average fuel temperature lower than the average moderator temperature can still be physical in some slices and are thus kept. With the state points shown in Table 6, the temperature ranges for the 30-MW case are 412–1566 K for the fuel and 294–1668 K for the moderator. For the 9-MW case, the temperature ranges for the fuel and the moderator are 329–835 K and 294–894 K, respectively. These extremum temperatures are obtained by applying the profile to the various state points for T_f and T_m and correspond to the values reached by the local fuel and moderator temperatures.

Table 6. Temperature table points selected for the cross-section functionalization in K for the 30-MW transient. Each temperature corresponds to the average; $T_f < T_m$ is thus not necessarily not physical.

T_m \ T_f	500	700	900	1100	1300	1500
400	✔	✔	✔	✔	✔	✔
600	✔	✔	✔	✔	✔	✔
800	✘	✔	✔	✔	✔	✔
1000	✘	✘	✔	✔	✔	✔
1200	✘	✘	✘	✔	✔	✔
1400	✘	✘	✘	✘	✔	✔

✔ means that the tabulation point has been calculated.
✘ means that this case is not physical.

Table 7. Temperature table points selected for the cross-section functionalization in K for the 9-MW transient.

T_m \ T_f	400	600	800
350	✔	✔	✔
550	✘	✔	✔
750	✘	✘	✔

✔ means that the tabulation point has been calculated.
✘ means that this case is not physical.

Each Serpent 2 case is run on Falcon using 10 full nodes (36 cores each). With 400 cycles of 2.5 million particles (plus 25 inactive cycles), a single calculation lasts less than 5 hours.

3.5   Poison Densities and Cross Sections

The library prepared for the LOFC transient is designed to separate the cross-section data between the contribution from the main neutron poisons and their precursors, namely I-135, Xe-135, Pm-149, and Sm-149, and the rest of the isotopes gathered into a residual term. In other words, the absorption, removal, transport, and total macroscopic cross sections are expressed as:

$$\Sigma_{x,g}(T_f, T_m) = \Sigma_{x,g}^{res}(T_f, T_m) + \sum_i \sigma_{x,g}^i(T_f, T_m)\, N_i(T_f, T_m) \tag{1}$$

where x represents the reaction type, g denotes the group index, Σ and σ are macroscopic and microscopic cross sections, respectively, i is the index looping over the four aforementioned neutron poisons and precursors and N_i is their respective atomic densities. For a given energy group and homogenization region, all of these quantities are assumed to only depend on T_f and T_m, the average fuel and moderator temperatures.

The idea is to use this library and only track the key isotopes with a depletion solver assuming that their microscopic cross sections are solely a function of the local fuel and moderator temperatures.

However, retrieving the poison microscopic cross sections in Serpent 2 requires to input the volume ratio of the fuel volume to the volume of the homogenized zone [15]. This is because the homogenized microscopic cross sections are evaluated as:

$$< \sigma_g > = \frac{1}{VR} \frac{\int_{E_g}^{E_{g-1}} dE \int_V \phi \sigma_g dx}{\int_{E_g}^{E_{g-1}} dE \int_V \phi dx}, \tag{2}$$

where, VR is the fuel volume ratio. The need for this extra coefficient is required because the poisons are only present in the fuel region making the denominator effectively zero in the non-fueled zone of the homogenized region. Unfortunately, the volume ratio is not identical for all blocks: Stacks 1 and 2 (see Figure 2) have 33 pins per block while Stacks 3 and 4 only have 31 pins. Therefore, these quantities are corrected through a post-processing script. Likewise, the atomic densities from Serpent 2 provided in the burned material output file correspond to the densities in the fuel and not in the block, meaning that they should also be corrected using the fuel volume ratio.

In the 9-MW case, the I-135 and Xe-135 equilibrium concentrations are obtained using a Serpent 2 feature, essentially assuming that the core was run to a 9-MW equilibrium and that the time required to do so did not significantly affect burnup. While this could potentially be a very impactful approximation, this is the best that can be done without knowing the exact power history. To compute the residual cross sections, the densities of Xe-135 in each universe are computed as the ratio of the macroscopic to the microscopic cross sections (both being provided by Serpent 2). For I-135, the atomic density is deduced from the following steady-state formulation:

$$I_{eq} = \frac{\gamma_I \sum_g \Sigma_{f,g} \phi_g}{\lambda_I V_b},$$ (3)

where I_{eq} is the equilibrium I-135 atomic density, γ_I is its fission yield, λ_I is its decay constant, and V_b is the volume of a block. Besides, $\Sigma_{f,g}$ and ϕ_g are the homogenized fission macroscopic cross section and the scalar flux integrated over the fuel block for energy group g, respectively.

4. MAMMOTH SPH CORRECTION

To gain confidence in the generated data, it is desired to evaluate the temperature coefficients and the power profile from MAMMOTH with and without SPH correction. The SPH factors are generated within MAMMOTH with two SPH regions per axial block. It should also be noted that these factors should only be applied using the same numerical parameters with which they have been generated, as any change in the numerical scheme or discretization is likely to affect them.
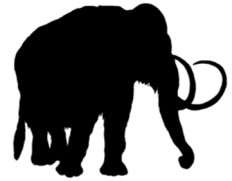
4.1 Eigenvalue and Temperature Coefficients

This section focuses on the multiplication factors obtained for each state point with and without SPH, as presented in Table 8 and Table 9. While the uncorrected results are between 1700 and 2050 pcm for the 30-MW case and between 2000 and 2200 pcm for the 9-MW, indicating a large homogenization error, the SPH correction enables to exactly reproduce the eigenvalues, which is a very significant improvement.

Table 8. MAMMOTH eigenvalues obtained with and without SPH correction compared to Serpent 2 for the 30-MW case.

T_f	T_m	Uncorrected keff	Uncorrected Error (pcm)	Corrected keff	Corrected Error (pcm)
500	400	1.10610	1911	1.08536	0
500	600	1.09652	1791	1.07722	0
700	400	1.08910	1946	1.06831	0
700	600	1.08123	1837	1.06173	0
700	800	1.07344	1761	1.05486	0
900	400	1.07337	1979	1.05254	0
900	600	1.06699	1872	1.04738	0
900	800	1.06037	1800	1.04162	0

Table 7. (continued).

T_f	T_m	Uncorrected keff	Uncorrected Error (pcm)	Corrected keff	Corrected Error (pcm)
900	1000	1.05376	1753	1.03561	0
1100	400	1.05866	1999	1.03792	0
1100	600	1.05368	1903	1.03400	0
1100	800	1.04805	1840	1.02911	0
1100	1000	1.04213	1798	1.02373	0
1100	1200	1.03621	1742	1.01847	0
1300	400	1.04520	2021	1.02449	0
1300	600	1.04129	1930	1.02157	0
1300	800	1.03651	1879	1.01739	0
1300	1000	1.03126	1833	1.01270	0
1300	1200	1.02576	1785	1.00777	0
1300	1400	1.01978	1715	1.00259	0
1500	400	1.03278	2046	1.01207	0
1500	600	1.02983	1961	1.01003	0
1500	800	1.02568	1914	1.00642	0
1500	1000	1.02100	1873	1.00223	0
1500	1200	1.01591	1827	0.99768	0
1500	1400	1.01022	1761	0.99274	0
Average		N/A	1864	N/A	

Table 9. MAMMOTH eigenvalues obtained with and without SPH correction compared to Serpent 2 for the 9-MW case.

T_f	T_m	Uncorrected keff	Uncorrected Error (pcm)	Corrected keff	Corrected Error (pcm)
400	350	1.05933	2132	1.03722	0
600	350	1.04139	2179	1.01919	0
600	550	1.03179	2053	1.01104	0
800	350	1.02483	2221	1.00256	0
800	550	1.01718	2099	0.996267	0
800	750	1.00957	2022	0.989561	0
Average		N/A	1864	N/A	

In addition, the moderator temperature coefficients for the 30-MW and 9-MW cases are compared in Table 10 and Table 11, respectively, for both the SPH uncorrected and corrected case. At a given fuel temperature T_f, it is defined as follows:

$$\alpha_{m,i}(T_f) = \frac{1}{T_{m,i} - T_{m,i-1}} \frac{k_i - k_{i-1}}{k_{i-1}}, \tag{4}$$

where i is the index of the moderator temperatures $T_{m,i}$ ordered contiguously such that for all i, j,

$$i < j \iff T_{m,i} < T_{m,j}. \tag{5}$$

The isothermal moderator coefficient from [24] is -2.8E-05 $\frac{\Delta k}{k}$/°C (unfortunately, the temperature at which it was evaluated is not specified). Thus, the uncorrected and corrected values obtained with MAMMOTH have reasonable values. Besides, it is no surprise that the error in the corrected case is zero since all the multiplication factors are exactly reproduced. However, it is significant in the uncorrected case. Worse, the relative error for the 30-MW case is not constant at different fuel temperatures, varying from -31% to almost 25%. At 9 MW, fewer points have been run but the relative error ranges from -11% to almost -19%. The fact that these relative errors vary noticeably implies that the non-SPH corrected case will suffer from significant reactivity feedback inaccuracy.

Table 10. Moderator temperature coefficients in $\frac{\Delta k}{k}$/°C from MAMMOTH with and without SPH correction compared to Serpent 2 for the 30-MW case.

T_f	T_m	Uncorrected α_m	Relative Error	Corrected α_m	Relative Error
500	400	-4.33E-05	-15.6%	-3.75E-05	0.0%
700	600	-3.61E-05	-17.3%	-3.08E-05	0.0%
700	800	-3.60E-05	-11.4%	-3.24E-05	0.0%
900	600	-2.97E-05	-21.2%	-2.45E-05	0.0%
900	800	-3.10E-05	-12.8%	-2.75E-05	0.0%
900	1000	-3.11E-05	-8.0%	-2.88E-05	0.0%
1100	600	-2.35E-05	-24.7%	-1.89E-05	0.0%
1100	800	-2.67E-05	-13.0%	-2.36E-05	0.0%
1100	1000	-2.82E-05	-7.9%	-2.61E-05	0.0%
1100	1200	-2.84E-05	-10.7%	-2.57E-05	0.0%
1300	600	-1.87E-05	-31.1%	-1.43E-05	0.0%
1300	800	-2.30E-05	-12.2%	-2.05E-05	0.0%
1300	1000	-2.53E-05	-9.9%	-2.30E-05	0.0%
1300	1200	-2.67E-05	-9.5%	-2.43E-05	0.0%
1300	1400	-2.92E-05	-13.4%	-2.57E-05	0.0%
1500	600	-1.43E-05	24.4%	-1.89E-05	0.0%
1500	800	-2.01E-05	14.8%	-2.36E-05	0.0%
1500	1000	-2.28E-05	12.7%	-2.61E-05	0.0%
1500	1200	-2.49E-05	3.0%	-2.57E-05	0.0%
1500	1400	-2.80E-05	4.5%	-2.93E-05	0.0%

Table 11. Moderator temperature coefficients in $\frac{\Delta k}{k}$/°C from MAMMOTH with and without SPH correction compared to Serpent 2 for the 9-MW case.

T_f	T_m	Uncorrected α_m	Relative Error	Corrected α_m	Relative Error
600	550	-4.61E-05	-15.3%	-4.00E-05	0.0%
800	550	-3.73E-05	-18.9%	-3.14E-05	0.0%
800	750	-3.74E-05	-11.1%	-3.37E-05	0.0%

Likewise, if the fuel temperature coefficients are defined at a given moderator temperature T_m as:

$$\alpha_{f,i}(T_m) = \frac{1}{T_{f,i}-T_{f,i-1}}\frac{k_i-k_{i-1}}{k_{i-1}}, \tag{6}$$

with the fuel temperatures $T_{f,i}$ ordered in the same way as before, then very similar conclusions can be drawn: all the values are reasonably close to -4.0E-05 $\frac{\Delta k}{k}$/°C, the isothermal fuel coefficient in [24] (unfortunately, the temperature at which it was evaluated is not specified). In addition, the corrected case reduces the error from between 2 and 5% to 0%, as shown in Table 12 and Table 13. Once again, having a varying relative error means that the fuel temperature feedback is inaccurate for the uncorrected case, though the variation is not as severe as for the moderator temperature feedback.

Table 12. Fuel temperature coefficients in $\frac{\Delta k}{k}$/°C from MAMMOTH with and without SPH correction compared to Serpent 2 for the 30-MW case.

T_f	T_m	Uncorrected α_f	Relative Error	Corrected α_f	Relative Error
700	400	-7.69E-05	2.2%	-7.85E-05	0.0%
900	400	-7.22E-05	2.1%	-7.38E-05	0.0%
1100	400	-6.85E-05	1.4%	-6.95E-05	0.0%
1300	400	-6.36E-05	1.7%	-6.47E-05	0.0%
1500	400	-5.94E-05	2.0%	-6.06E-05	0.0%
700	600	-6.97E-05	3.0%	-7.19E-05	0.0%
900	600	-6.59E-05	2.5%	-6.76E-05	0.0%
1100	600	-6.24E-05	2.4%	-6.39E-05	0.0%
1300	600	-5.88E-05	2.2%	-6.01E-05	0.0%
1500	600	-5.50E-05	2.6%	-5.65E-05	0.0%
900	800	-6.09E-05	3.0%	-6.28E-05	0.0%
1100	800	-5.81E-05	3.3%	-6.01E-05	0.0%
1300	800	-5.50E-05	3.3%	-5.69E-05	0.0%
1500	800	-5.22E-05	3.1%	-5.39E-05	0.0%
1100	1000	-5.52E-05	3.8%	-5.74E-05	0.0%
1300	1000	-5.22E-05	3.1%	-5.39E-05	0.0%
1500	1000	-4.97E-05	3.8%	-5.17E-05	0.0%
1300	1200	-5.04E-05	4.0%	-5.25E-05	0.0%
1500	1200	-4.80E-05	4.1%	-5.01E-05	0.0%
1500	1400	-4.69E-05	4.6%	-4.91E-05	0.0%

Table 13. Fuel temperature coefficients in $\frac{\Delta k}{k}$/°C from MAMMOTH with and without SPH correction compared to Serpent 2 for the 9-MW case.

T_f	T_m	Uncorrected α_f	Relative Error	Corrected α_f	Relative Error
600	350	-8.46E-05	2.6%	-8.69E-05	0.0%
800	350	-7.95E-05	2.5%	-8.16E-05	0.0%
800	550	-7.08E-05	3.1%	-7.31E-05	0.0%

In summary, the SPH correction is very important to reproduce the temperature feedback accurately.

4.2   Power Profile

Because multiplication factors (and thus reactivity coefficients) are defined using spatially integrated quantities, reproducing them is necessary but not sufficient to conclude that the reference solution is accurately represented. In this section, the spatial error in the power of the MAMMOTH solution is compared to the Serpent 2 calculation using the following figures of merit:

$$\text{RMS} = \sqrt{\frac{1}{V}\sum_i V_i \left(\frac{P_i - P_i^{ref}}{P_i^{ref}}\right)^2} \quad , \quad \text{MAX} = \max_i \left(\frac{P_i - P_i^{ref}}{P_i^{ref}}\right) \quad , \quad \text{MIN} = \min_i \left(\frac{P_i - P_i^{ref}}{P_i^{ref}}\right),$$

where V is the total fuel volume, i is the index of the SPH region of volume V_i, P_i and P_i^{ref} are the MAMMOTH and Serpent 2 powers of that region, respectively.

Table 14 and Table 15 show these quantities in the uncorrected and corrected case for the 30-MW and 9-MW cases, respectively. Although the MAMMOTH and Serpent 2 calculations are normalized to the same power, the uncorrected case shows significant differences, with a root mean square (RMS) averaging almost 3% and extrema of almost 6% in certain SPH regions for the 30-MW case. With a 9-MW power, the average RMS is above 4.2% with extremum values reaching over 14%. This means that the power profile accuracy is even worse in the 9-MW case if SPH is not applied.

On the other hand, the corrected case shows extremely good results: the RMS, MAX, and MIN are all smaller than without SPH by about a factor 30 or more, confirming that the SPH procedure drastically reduces the homogenization error and should thus be decisive in accurately capturing the recriticality time of the LOFC transient.

Table 14. MAMMOTH error in power profile with and without SPH correction for the 30-MW case.

T_f	T_m	Uncorrected			Corrected		
		RMS	MAX	MIN	RMS	MAX	MIN
500	400	2.96%	6.53%	-5.14%	0.09%	0.23%	-0.25%
500	600	3.01%	6.16%	-5.54%	0.08%	0.19%	-0.21%
700	400	2.95%	6.44%	-5.17%	0.08%	0.20%	-0.17%
700	600	3.00%	6.04%	-5.50%	0.08%	0.18%	-0.21%
700	800	2.98%	5.95%	-5.45%	0.07%	0.16%	-0.18%
900	400	2.93%	6.38%	-5.13%	0.09%	0.25%	-0.24%
900	600	2.96%	6.09%	-5.39%	0.07%	0.16%	-0.16%
900	800	2.93%	6.06%	-5.29%	0.07%	0.16%	-0.15%
900	1000	2.96%	5.76%	-5.42%	0.06%	0.14%	-0.17%

Table 13. (continued).

T_f	T_m	Uncorrected			Corrected		
		RMS	MAX	MIN	RMS	MAX	MIN
1100	400	2.93%	6.42%	-5.16%	0.08%	0.19%	-0.22%
1100	600	2.97%	6.25%	-5.37%	0.08%	0.21%	-0.18%
1100	800	2.92%	5.96%	-5.23%	0.08%	0.20%	-0.21%
1100	1000	2.95%	5.82%	-5.36%	0.08%	0.22%	-0.18%
1100	1200	3.03%	5.64%	-5.73%	0.08%	0.18%	-0.17%
1300	400	2.93%	6.31%	-5.23%	0.09%	0.21%	-0.27%
1300	600	2.96%	6.09%	-5.23%	0.08%	0.17%	-0.18%
1300	800	2.90%	5.90%	-5.27%	0.07%	0.20%	-0.16%
1300	1000	2.93%	5.86%	-5.29%	0.07%	0.17%	-0.16%
1300	1200	2.99%	5.66%	-5.58%	0.07%	0.17%	-0.20%
1300	1400	3.12%	5.38%	-6.20%	0.07%	0.20%	-0.16%
1500	400	2.94%	6.30%	-5.28%	0.08%	0.20%	-0.19%
1500	600	2.93%	6.22%	-5.14%	0.08%	0.22%	-0.19%
1500	800	2.91%	6.00%	-5.23%	0.07%	0.19%	-0.17%
1500	1000	2.92%	5.82%	-5.20%	0.07%	0.18%	-0.19%
1500	1200	2.97%	5.60%	-5.53%	0.07%	0.16%	-0.18%
1500	1400	3.08%	5.49%	-6.02%	0.07%	0.17%	-0.20%
	Max	3.12%	6.53%	-6.20%	0.09%	0.25%	-0.27%
	Average	2.96%	6.00%	-5.39%	0.08%	0.19%	-0.19%

Table 15. MAMMOTH error in power profile with and without SPH correction for the 9-MW case.

T_f	T_m	Uncorrected			Corrected		
		RMS	MAX	MIN	RMS	MAX	MIN
400	350	4.22%	13.89%	-10.65%	0.10%	0.28%	-0.42%
600	350	4.24%	14.08%	-10.65%	0.09%	0.32%	-0.32%
600	550	4.18%	14.46%	-10.41%	0.08%	0.24%	-0.30%
800	350	4.28%	14.13%	-10.94%	0.10%	0.34%	-0.41%
800	550	4.21%	14.43%	-10.70%	0.09%	0.28%	-0.31%
800	750	4.22%	14.26%	-10.59%	0.09%	0.26%	-0.30%
	Max	4.28%	14.46%	-10.94%	0.10%	0.34%	-0.42%
	Average	4.24%	14.24%	-10.70%	0.09%	0.29%	-0.35%

5. CONCLUSION

In summary, a 3-D Serpent 2 model of the HTTR was developed to generate homogenized neutron cross sections as a function of the fuel and moderator temperatures with the intent to simulate the 9-MW and 30-MW LOFC transients. This model agreed very closely to a previous MCNP6 model. Failure to account for the temperature profile within the core led to significant errors, especially due to the strong axial temperature gradients. A temperature model was developed with the shape assumed to be time-independent and tabulated 3-D cross-sections were generated at 390 EFPDs so that the tabulation points would bound the range of all physical temperatures that could occur in the transient. Since the poison concentrations and the control rod positions differed based on the initial power of the LOFC, separate libraries were constructed for the 9-MW and 30-MW LOFCs. MAMMOTH was used to evaluate the homogenization error resulting from these cross sections, which was determined to be quite large, in terms of multiplication factors, reactivity coefficients, and power profile. The SPH procedure from MAMMOTH was then deployed and excellent agreement resulted, reaching 0 pcm error for the eigenvalue and less than 0.1% error in the RMS of the power profile.

However, it is recommended that future work includes the local burnup to functionalize the cross sections. This will allow capture of the local effects of the core during the depletion to obtain improved cross section accuracy when using a more accurate temperature profile produced by high-fidelity multiphysics codes. It is also planned to use MAMMOTH coupled to BISON and RELAP-7 to simulate this HTTR LOFC to simultaneously simulate neutronics, depletion, thermal radiation, and thermal-hydraulics.

6. REFERENCES

1. S. Shiozawa, S. Fujikawa, T. Iyoku, K. Kunitomi, Y. Tachibana, "Overview of HTTR design features," *Nuclear Engineering and Design*, Vol. 233, pp. 11–21, 2004.

2. F. Akino, M. Takeuchi, T. Ono, and Y. Kaneko, "Experimental Verification and Analysis of Neutron Streaming Effect through Void Holes for Control Rod Insertion in HTTR," *Journal of Nuclear Science and Technology*, Vol. 34, No.2, pp. 185–192, February 1997.

3. J. C. Kuijper, X. Raepsaet, J. B. M. de Haas, W. von Lensa, U. Ohlig, H. –J. Ruetten, H. Brockmann, F. Damian, F. Dolci, W. Bernnat, J. Oppe, J. L. Kloosterman, N. Cerullo, G. Lomonaco, A. Negrini, J. Magill, R. Seiler, "HTGR reactor physics and fuel cycle studies," *Nuclear Engineering and Design*, Vol. 236, pp. 615–634, March 2006.

4. S. Nakagawa, Y. Tachibana, K. Takamatsu, S. Ueta, S. Hanawa, "Performance test of HTTR," *Nuclear Engineering and Design*, Vol. 233, pp. 291–300, October 2004.

5. T. Shibata, T. Kikuchi, S. Miyamoto, and K. Ogura, "Assessment of Irradiation Temperature Stability of the First Irradiation Test Rig in the HTTR," *Nuclear Engineering and Design*, Vol. 23, pp. 133–143, 2003.

6. Y. Tachibana, S. Nakagawa, T. Takeda, A. Saikusa, T. Furusawa, K. Takamatsu, K. Sawa, and T. Iyoku, "Plan for the First Phase of Safety Demonstration Tests of the High Temperature Engineering Test Reactor (HTTR)," *Nuclear Engineering and Design*, Vol. 224, pp. 179–197, 2003.

7. S. Nakagawa, K. Takamatsu, Y. Tachibana, N. Sakaba, and T. Iyoku, "Safety Demonstration Tests using High Temperature Engineering Test Reactor," *Nuclear Engineering and Design*, Vol. 233, pp. 301–308, 2004.

8. J. Bess, N. Fujimoto, B. Dolphin, L. Snoj, A. Zukeran, *Evaluation of the Start-Up Core Physics Tests at Japan's High Temperature Engineering Test Reactor (Fully-Loaded Core)*, INL/EXT-08-14767, March 2009.

9. J. Bess, N. Fujimoto, J. Sterbentz, L. Snoj, A. Zukeran, *Evaluation of the Start-Up Core Physics Tests at Japan's High Temperature Engineering Test Reactor (Annular Core Loadings)*, INL/EXT-09-15794, March 2010.

10. J. Bess, N. Fujimoto, J. Sterbentz, L. Snoj, A. Zukeran, *Evaluation of Zero-Power, Elevated Temperature Measurements at Japan's High Temperature Engineering Test Reactor*, INL/EXT-10-19627, March 2011.

11. ORNL, 2009, *SCALE: A Modular Code System for Performing Standardized Computer Analyses for Licensing Evaluations*, ORNL/TM-2005/39, Version 6, Vols, I-III, Oak Ridge National Laboratory, January 2009.

12. G. Marleau, A. Hébert, and R. Roy, *A User Guide for Dragon Version5*, Technical Report IGE-335, Ecole Polytechnique de Montreal, 2016.

13. J. Ortensi, J. Cogliati, M. Pope, J. Bess, R. Ferrer, A. Bingham, A. Ougouag, *Deterministic Modeling of the High Temperature Test Reactor*, INL/EXT-10-18969, June 2010.

14. S. Sen, A. Hummel, and H. Hiruta, *Super-Homogenization-Corrected Cross-Section Generation for High-Temperature Reactors*, INL/EXT-17-41516, March 2017.

15. J. Leppanen, et al., "The Serpent Monte Carlo code: Status, development and applications in 2013," *Annals of Nuclear Energy*, Vol. 82, pp. 142–150, 2015.

16. A. Hébert. "Développement de la méthode SPH: Homogénéisation de cellules dans un réseau non uniforme et calcul des paramètres de réflecteur," Ph.D. thesis, CEA-N2209, 1981.

17. J. Ortensi, Y. Wang, A. Laurier, S. Schunert, A. Hébert, and M. DeHart, "A Newton Solution for the Superhomogenization Method: The PJFNK-SPH," *Annals of Nuclear Energy*, Vol. 111, pp. 579–594, January 2018.

18. X-5 Monte Carlo Team, "MCNP – A General Monte Carlo N-Particle Transport Code, Version 5, Volume 1: Overview and Theory," Los Alamos National Laboratory, LA-UR-03-1987, 2003.

19. K. Takamatsu, X. Yan, S. Nakagawa, and N. Sakaba, "Spontaneous stabilization of HTGRs without reactor scram and core cooling – Safety demonstration tests using the HTTR: Loss of reactivity control and core cooling," *Nuclear Engineering and Design,* Vol. 271, pp. 379–387, 2014.

20. F. Gleicher, J. Ortensi, et al., "The Coupling of the Neutron Transport Application RATTLESNAKE to the Fuels Performance Application BISON," in "International Conference on Reactor Physics (PHYSOR 2014)," Kyoto, Japan, May 2014.

21. D. Gaston, C. Newman, G. Hansen, and D. Lebrun-Grandié, "MOOSE: A Parallel Computational Framework for Coupled Systems of Nonlinear Equations," *Nuclear Engineering and Design*, Vol. 239, No. 10, pp. 1768–1778, 2009.

22. Benjamin A. Baker, Javier Ortensi, Mark D. DeHart, Yaqi Wang, Sebastian Schunert, and Frederick N. Gleicher, "Analysis Methods and Validation Activities for MAMMOTH Using M8 Calibration Series Data," INL/EXT-16-40023, September 2016.

23. R. Baker, G. Strydom, "Civil Nuclear Energy Working Group Project: High Temperature Engineering Test Reactor Transient Simulation with PHISICS/RELAP5-3D," December 2016.

24. N. Sakaba, et. al., "Safety Demonstration Test (SR-2/S2C-2/SF-1) Plan using the HTTR," JAERI-Tech 2004-014.